SCIENCE CHINA
Information Sciences

• RESEARCH PAPER •

May 2024, Vol. 67, Iss. 5, 152304:1–152304:11
https://doi.org/10.1007/s11432-023-3912-0

Low-resolution Kramers-Kronig detection system with error-feedback noise shaping

Xiangyong DONG, Zhenming YU*, Hongyu HUANG, Kaixuan SUN & Kun XU

State Key Laboratory of Information Photonics and Optical Communications, Beijing University of Posts and Telecommunications, Beijing 100876*, China*

Received 20 June 2023/Revised 14 October 2023/Accepted 7 December 2023/Published online 25 April 2024

Abstract In this paper, we investigated the effects of error-feedback noise shaping (EFNS) on a low-resolution Kramers-Kronig (KK) detection system for the first time. Both 16-ary quadrature amplitude modulation (16-QAM) and 64-ary quadrature amplitude modulation (64-QAM) were considered in the experiment. The carrier tone was added on the transmitter side using the virtual carrier-assisted single sideband (VCA-SSB) method to meet the minimum phase (MP) condition. Under the MP condition, KK detection only needs the intensity of the optical signal to be detected by one photodiode (PD) to retrieve the phase information. However, the virtual carrier tone increases the carrier-to-signal power ratio (CSPR), which results in a high peak-to-average power ratio (PAPR) at the transmitter, causing an increase in quantization noise. To mitigate quantization noise in the low-resolution KK detection system, EFNS was applied. The application of EFNS increased the optimal CSPR of the KK detection system and improved receiver sensitivity. Using a 4-bit DAC and the EFNS, 80 km transmission was achieved in the 60-Gbit/s 64-QAM KK detection system.

Keywords optical fiber communications, Kramers-Kronig receiver, error-feedback noise shaping, quantization noise, carrier-to-signal power ratio

1 Introduction

In recent years, the demand for low-cost optical transmission systems has grown significantly due to the vital role they play in emerging cost-sensitive applications, such as data center interconnects (DCIs) and metro-area networks [1–3]. With the rapid development of digital signal processing (DSP) technology, the Kramers-Kronig (KK) receiver [4] has been proposed as a low-cost self-coherent receiver, garnering extensive interest from the field of optical metro networks research [5–7].

The KK receiver demonstrates exceptional capabilities in mitigating signal-to-signal beat interference (SSBI) [8] and effectively reconstructing the complex optical field of a minimum phase (MP) signal using only a single photodiode [4, 9]. The MP signal consists of the signal and the carrier tone at the edge of the signal spectrum. The carrier tone required for the MP signal can be added in different ways. For example, the carrier tone can be induced by the direct current (DC) bias of the dual-driver Mach-Zehnder modulator [6, 10, 11]. Although this method is simple, it requires generating the SSB signal at the transmitter, which doubles the required electrical bandwidth. Alternatively, the carrier tone can be added to the optical field by an extra laser or polarization-maintaining coupler (PMC) [12,13]. The carrier tone can also be added via the digital method, which is named the virtual carrier-assisted single sideband (VCA-SSB) method [14–16]. The VCA-SSB method generates a digital tone that acts as a virtual carrier, together with the transmitted signal at the transmitter. Compared to previous methods, the VCA-SSB method is simple but practical and requires no extra hardware overhead. However, the VCA-SSB method increases the peak-to-average power ratio (PAPR) of the digital signal at the transmitter and raises the quantization noise of the digital-to-analog converter (DAC).

Error-feedback noise shaping (EFNS) has gained significant attention in the realm of low-resolution transmission systems due to its advantageous characteristics of low complexity and no processing

* Corresponding author (email: yuzhenming@bupt.edu.cn)

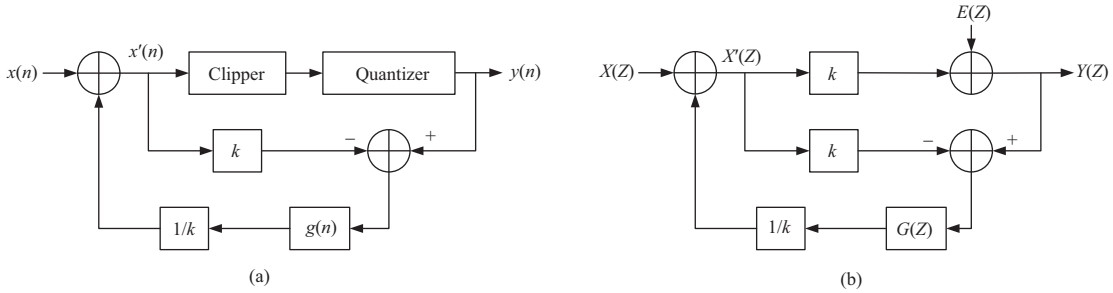

Figure 1 Schematic of the EFNS principle. (a) Time-domain model; (b) Z-domain model.

delay [17–19]. EFNS is based on linear models of quantization and clipping [20]. It shapes the quantization noise from the frequency domain to reduce the quantization noise inside the signal band and to improve the effective resolution of the DAC.

In this paper, we investigated the effects of the EFNS algorithm on a low-resolution KK detection system for the first time. We experimentally transmitted 56-Gbit/s 16-QAM signals and 60-Gbit/s 64-QAM signals in optical back-to-back (OB2B) transmission and 80 km standard single-mode fiber (SSMF) transmission. The physical numbers of bits (PNoBs) used in the experiments were 4, 5, and 8. First, we performed a simulation-based analysis to investigate the effectiveness of EFNS in mitigating the increased quantization noise caused by the addition of the virtual carrier at the transmitter. Subsequently, an experimental investigation was conducted to evaluate the impact of EFNS on a low-resolution KK detection system from three perspectives: CSPR, AWG output amplitude, and received optical power (ROP). Furthermore, we conducted an analysis of the synergistic effects of EFNS and KK detection on system performance, considering the increased optimal CSPR achieved by EFNS. This analysis highlights the dual benefits of EFNS, as it not only enhances overall system performance but also contributes to the improved performance of KK detection, thereby further enhancing system performance. Three cases were analyzed:

Case 1. Under the optimal CSPR without EFNS, only KK detection is employed in the transmission system.

Case 2. Under the optimal CSPR without EFNS, KK detection combined with EFNS is employed in the transmission system.

Case 3. Under the optimal CSPR with EFNS, KK detection combined with EFNS is employed in the transmission system.

Compared to the first two cases, Case 3 showed the best performance at its optimal CSPR.

This paper is organized as follows: Section 2 illustrates the principles of EFNS. Section 3 specifies the impact of the EFNS algorithm on the transmitter of the VCA-SSB KK detection transmission system. Section 4 presents the experimental setup. Section 5 discusses the experimental results. Finally, Section 6 presents the conclusions.

2 Error-feedback noise shaping

EFNS is a noise-shaping technique based on a quantized linear model that can simultaneously shape clipping and quantization noise [20]. The noise-shaping function of EFNS is mainly realized by loop filtering, as shown in Figure 1(a).

When the input does not exceed the input range of the quantizer and satisfies the quantization theorem [21], the quantization error can be considered additive white noise, independent of the input [20]. Thus, we can obtain the following:

$$x_q(n) = x(n) + e_q(n), \tag{1}$$

where $x_q(n)$ and $e_q(n)$ are the output and quantization noise of the quantizer, respectively. In addition to the quantified linear model, EFNS uses a clipping-quantified model. When the mean input value of clipping is zero and satisfies the Gaussian distribution, the linear clipping model can be derived based on Bussgang's theorem. The linear clipping model is as follows [20]:

$$\begin{cases} x_c(n) = kx(n) + e_c(n), \\ k = \mathrm{cov}(x_c, x)/\mathrm{Var}(x), \end{cases} \tag{2}$$

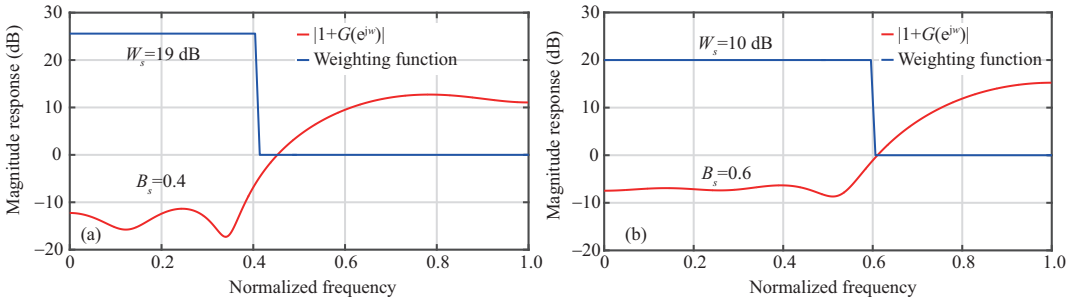

Figure 2 (Color online) Weighting function and corresponding noise-shaping (NS) function. (a) Parameters for the simulation: $W_s = 19$ dB, $B_s = 0.4$; (b) parameters for the experiment: $W_s = 10$ dB, $B_s = 0.6$.

where $x_c(n)$ and $e_c(n)$ denote the output and noise of clipping, respectively. k is the scaling factor of the clipper. $\mathrm{Cov}(\cdot,\cdot)$ means covariance, and $\mathrm{Var}(\cdot)$ denotes the variance. When clipping is not used, k is equal to 1 and EFNS is similar to a delta-sigma DAC with an error-feedback structure. According to Eqs. (1) and (2), the Z-domain model of EFNS can be obtained, as shown in Figure 1(b). The Z-domain transfer function of EFNS is expressed as follows [20]:

$$Y(z) = KX'(z) + E(z) = kX(z) + (1 + G(z))E(z), \tag{3}$$

$$E(z) = E_q(z) + E_z(z). \tag{4}$$

Eq. (3) shows that the spectrum of clipping and quantization noise can be shaped by adjusting $1+G(z)$. $G(z)$ is usually a finite impulse response (FIR) filter. Its coefficient can be calculated by minimizing the following equation [19]:

$$\int_{\Omega} |W(\mathrm{e}^{\mathrm{j}\omega})(1 + G(\mathrm{e}^{\mathrm{j}\omega}))|^2 \mathrm{d}\omega, \tag{5}$$

where $W(\mathrm{e}^{\mathrm{j}\omega})$ is the weighting function, and Ω is the sampling band of DAC. To achieve a good quantization noise-shaping effect, the weight function should be larger in the signal frequency band and smaller in the unused frequency band. In general, the weight in the unused band is set to 1. The weight in the signal band W_s and the cut-off frequency B_s of the weight function should be carefully optimized according to the effect of quantization noise shaping. Figure 2(a) shows the values of W_s and B_s in the simulation. Figure 2(b) shows the values of W_s and B_s in the experiments.

3 Impact of EFNS at the transmitter of the VCA-SSB KK detection transmission system

In KK detection, it is essential for the signal to meet the MP condition to guarantee effective reconstruction [4]. The MP condition requires that the power of the carrier tone be sufficiently high, which means that the CSPR should be sufficiently high. CSPR is the power ratio between the signal and carrier power, which is given by the following:

$$\mathrm{CSPR} = \frac{P_{\mathrm{carrier}}}{P_{\mathrm{signal}}}, \tag{6}$$

where P_{carrier} and P_{signal} represent the power of the carrier tone and signal, respectively. The carrier tone is added by the VCA-SSB method at the transmitter side [16]. Additionally, the amplitude of the virtual carrier tone can be varied to attain the desired CSPR. Since the number of output levels available for the DAC is fixed, the number of quantization levels available for the quantization signal depends on the CSPR. When the CSPR is increased, the number of quantization levels available for the signal is reduced, which leads to an increase in quantization noise.

Figure 3 describes the relationship between CSPR and the transmitter signal-to-noise ratio (SNR) for 5-bit DAC in the 112-Gbit/s 16-QAM simulation OB2B transmission, where only quantization noise is considered as noise source at the transmitter. In the low CSPR range, the curves are relatively flat, indicating that the inherent quantization noise of the system predominantly limits the transmitter SNR. As the CSPR increases, the PAPR increases in the high CSPR range, inducing more quantization noise and reducing the SNR at the transmitter. The results imply that the increase in CSPR adversely affects

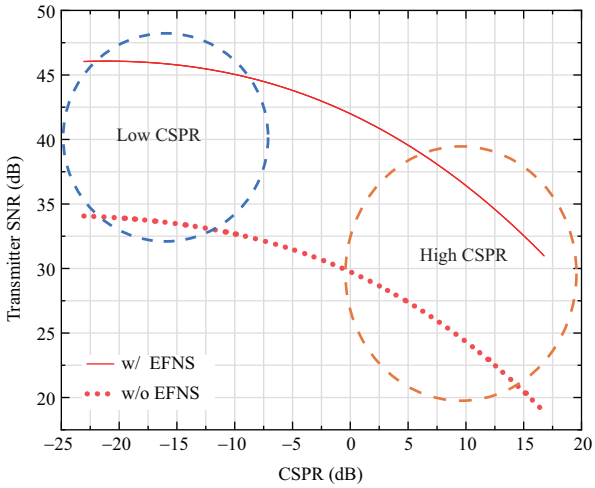

Figure 3 (Color online) Simulation results of the transmitter SNR versus CSPR in 16-QAM OB2B transmission with a 5-bit DAC.

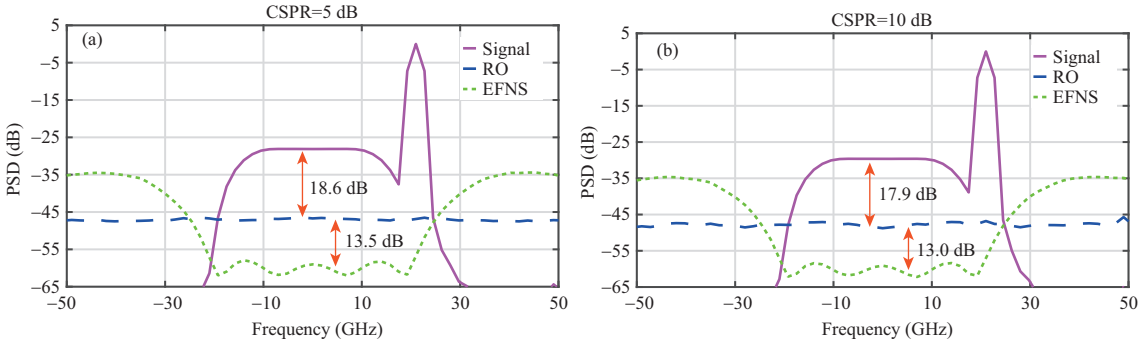

Figure 4 (Color online) Simulated spectrums of the signal and quantization noise of round-off (RO) quantization and EFNS with a 5-bit DAC in different CSPRs. (a) CSPR = 5 dB; (b) CSPR = 10 dB.

the signal quality at the transmitter. However, by applying EFNS, the transmitter SNR can be enhanced to alleviate the impact of CSPR on the signal quality at the transmitter.

The effect of EFNS on the quantization noise at different CSPR values is depicted in Figure 4. This shows that the quantization noise of the round-off (RO) quantization is flat. When the CSPR is increased, the quantization noise is increased to degrade the quality of the transmitted signal. Figure 4 also shows that when EFNS is applied, the quantization noise power is reduced at low frequency and increased at high frequency to reduce the quantization noise within the signal band. Notably, irrespective of the CSPR values, the EFNS can limit the quantization noise to a relatively low value to mitigate the deterioration of the transmitted signal.

In addition, although the increase in the CSPR degrades signal quality at the transmitter, it decreases the SSBI of the received signal and enhances the signal reconstruction capability of KK detection [8]. Thus, there exists an optimal CSPR for the KK detection system. The application of EFNS alleviates the deterioration of the transmitted signal caused by the increase in the CSPR, which means that enabling EFNS is expected to increase the optimal CSPR of the KK detection system and contribute to reducing the SSBI in the KK detection system.

4 Experimental setup

To experimentally validate the effects of EFNS on the low-resolution KK detection system, we conducted experiments of 80 km KK detection systems as shown in Figure 5(a). The DSP flow in the transmitter is shown in Figure 5(b), where the roll-off factor of the square-root-raised cosine (SRRC) filter is 0.01. In the experiment, an optical carrier with wavelengths of 1550 nm was injected into the in-phase and quadrature Mach-Zehnder modulator (IQ-MZM, FTM7962EP/301) biased at its transmission null. The signals were

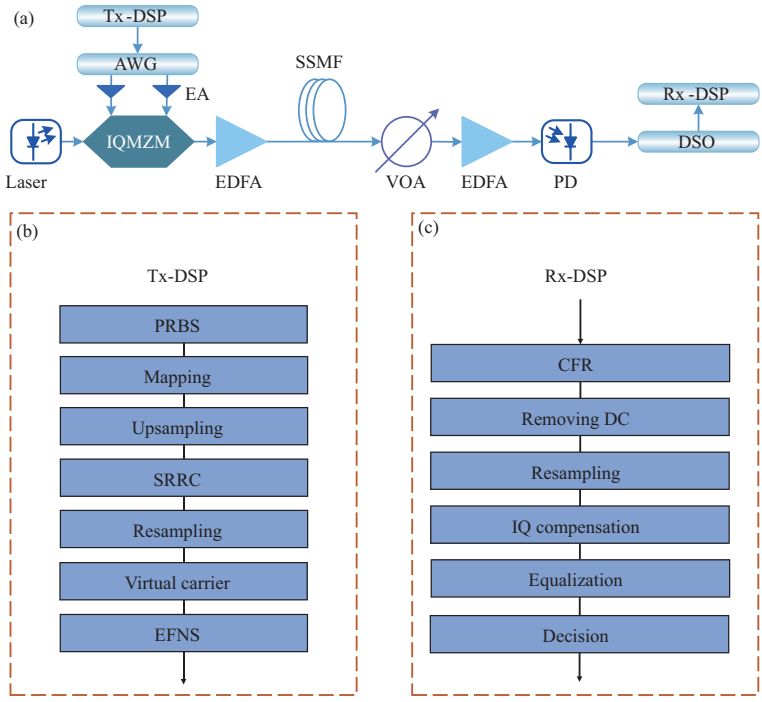

Figure 5 (Color online) (a) Experimental setup for low-resolution 16-QAM and 64-QAM KK detection systems; (b) transmitter DSP flow; (c) receiver DSP flow. PRBS: pseudo-random binary sequence.

generated by an arbitrary waveform generator (AWG, Keysight M8195A). The highest sampling rate and analog bandwidth of this AWG were 65 GSa/s and 25 GHz, respectively. The electrical analog signals generated by the AWG were amplified using an electric amplifier (EA). The signals were then modulated by the IQ-MZM and transmitted through an 80 km standard single-mode fiber (SSMF). At the receiver side, the optical signals were detected by a DC coupling photodiode (PD). The electrical signals from the PD were digitized and captured by a 100 GSa/s digital sampling oscilloscope (DSO) with an analog bandwidth of 25 GHz (Tektronix DSA72504D). The digital signals were then processed by the receiver DSP. To ensure the accurate complex field reconstruction (CFR), a resampling rate of four is used before going through the KK algorithm. After the KK algorithm, the data streams are then resampled to two samples per symbol for the following DSP flow. The DSP flow in the receiver is shown in Figure 5(c).

Two modulation formats of 16-QAM and 64-QAM were considered in the experiments, respectively. In 56-Gbit/s KK-16-QAM transmission, the frequency shift of the virtual carrier was 8 GHz. In 60-Gbit/s KK-64-QAM transmission, the frequency shift of the virtual carrier was 6.5 GHz.

5 Experimental results and discussion

In this section, we discuss the experimental demonstrations of the impact of EFNS on low-resolution 16-QAM and 64-QAM KK detection systems with PNoBs of 4, 5, and 8. We analyzed the influence of EFNS on various aspects of the KK detection system, including CSPR, AWG output amplitude, and ROP. It is worth noting that we maintained the CSPRs at their respective optimal values for each transmission scenario when evaluating the effects of EFNS on AWG output amplitude and ROP.

5.1 VCA-SSB 56-Gbit/s KK-16-QAM transmission

First, we swept the CSPR for the VCA-SSB 56-Gbit/s KK-16-QAM transmission system in OB2B and 80 km SSMF transmission. The experimental results are shown in Figure 6.

In OB2B transmission, as shown in Figure 6(a), when PNoB = 4, the optimum CSPR was 9.28 dB, which is 1.94 dB higher than that when EFNS was not applied. Furthermore, the BER was reduced from 2.9×10^{-3} to 9.3×10^{-4}. And the required CSPR at the hard-decision forward error correction (HD-FEC) threshold was reduced by approximately 0.5 dB. When PNoB = 5, the results showed that the optimal CSPR was 10.86 dB, which is 1.58 dB higher than that when EFNS was not applied. Furthermore, the

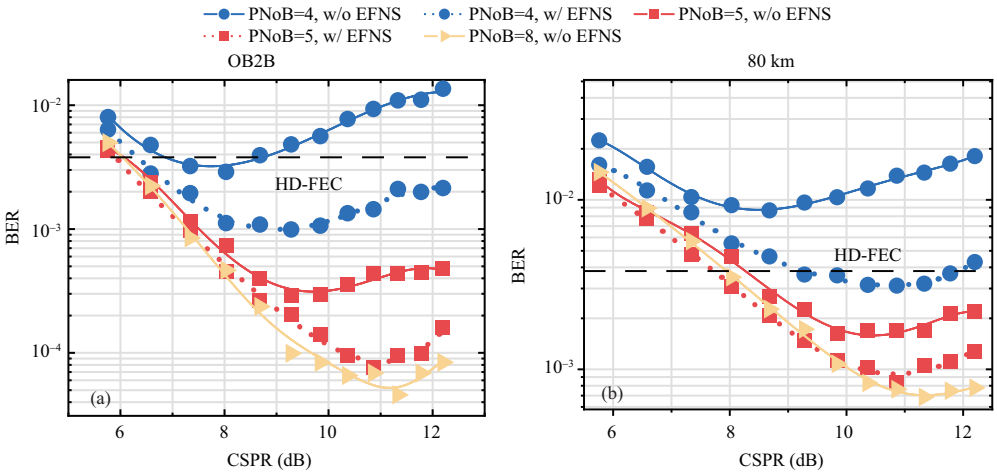

Figure 6 (Color online) CSPR versus BER in the VCA-SSB 56-Gbit/s KK-16-QAM transmission. (a) OB2B transmission; (b) 80 km SSMF transmission.

BER was reduced from 2.9×10^{-4} to 7.6×10^{-5}. Comparing the case of PNoB = 4 and PNoB = 5, the experimental results showed that the EFNS is more effective in the low-resolution KK detection system to improve the optimal CSPR of the KK receiver. When PNoB = 8, the optimal CSPR was 11.33 dB, and the BER was 4.6×10^{-5}. Comparing the case of PNoB = 5 and PNoB = 8, the experimental results illustrate that the optimal CSPR and BER performance of a 5-bit DAC KK detection system with EFNS can be improved, similar to that of an 8-bit DAC KK detection system. Figure 6(b) shows the experimental results of the 80 km transmission. The results showed that the system performance degraded compared to the results in Figure 6(a) due to the chromatic dispersion (CD) and channel loss of the 80 km SSMF. Furthermore, CD increased the PAPR of the received signal, which requires a higher CSPR for KK detection to be robust against CD [22]. When PNoB = 4, the optimal CSPR was 10.86 dB, which increased by 2.18 dB. The BER was decreased from 8.7×10^{-3} to 3.2×10^{-3}. The experimental results showed that by applying EFNS, the performance of the 4-bit DAC KK detection system met the HD-FEC threshold. When PNoB = 5, enabling the EFNS, the optimum CSPR was increased from 9.84 to 10.86 dB, increasing about 1.02 dB. The BER decreased from 1.6×10^{-3} to 7.9×10^{-4}. The required CSPR at the HD-FEC threshold was reduced by about 0.5 dB. When PNoB = 8, the optimal CSPR was 11.33 dB, and the BER was 7×10^{-4}. The experimental results in Figure 6 show that the optimum CSPR increased when EFNS was applied, and the performance also improved at the optimum CSPR. As explained in Section 3, when employing EFNS, the quantization noise in the high CSPR region is suppressed at a low value. This outcome indicates that applying EFNS increased the robustness of the system for high PAPRs. Consequently, it enables the KK detection system to operate with an elevated optimal CSPR.

Then, we swept the AWG output amplitude to determine the optimal AWG output amplitudes under different optimal CSPRs and evaluate the impact of EFNS on the AWG output amplitude. The BER performances at different AWG output amplitudes with OB2B transmission and 80 km transmission are plotted in Figures 7(a) and (b), respectively. In OB2B transmission with PNoB = 4, applying EFNS, the required AWG output amplitude was reduced by 70 mV at the HD-FEC threshold. When PNoB = 5, the required AWG output amplitude still decreased at the HD-FEC threshold. In 80 km transmission, applying EFNS, the BER performance of PNoB = 4 met the HD-FEC threshold. When PNoB = 5, the required AWG output amplitude was reduced by 10 mV. The results in Figure 7 show that applying EFNS resulted in smaller AWG output amplitudes required for the KK detection system.

Next, at the optimal CSPRs, the impact of EFNS on the ROP was experimentally analyzed, as shown in Figure 8. Figure 8(a) shows that when PNoB = 4, applying EFNS, the required ROP decreased by 5.9 dBm at the HD-FEC threshold. When PNoB = 5, the required ROP decreased by 0.6 dBm at the HD-FEC threshold. Comparing the results of PNoB = 4 and PNoB = 5, the experimental results showed that EFNS was more effective in improving the receiver sensitivity of the KK detection system in the case of low resolution. In 80 km transmission, the experimental results showed that when PNoB = 4, applying EFNS, the BER performance met the HD-FEC threshold at the ROP of −16.9 dBm. When PNoB = 5, the required ROP was reduced by 1 dBm at the HD-FEC threshold.

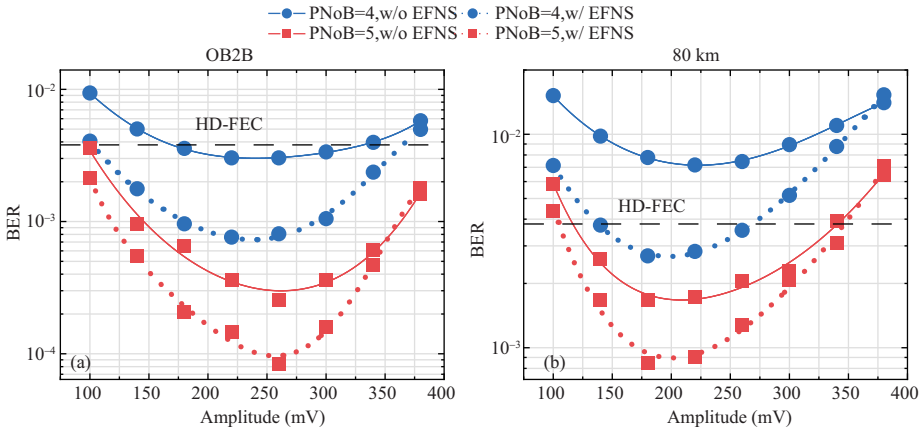

Figure 7 (Color online) AWG output amplitude versus BER in the VCA-SSB 56-Gbit/s KK-16-QAM transmission. (a) OB2B transmission; (b) 80 km SSMF transmission.

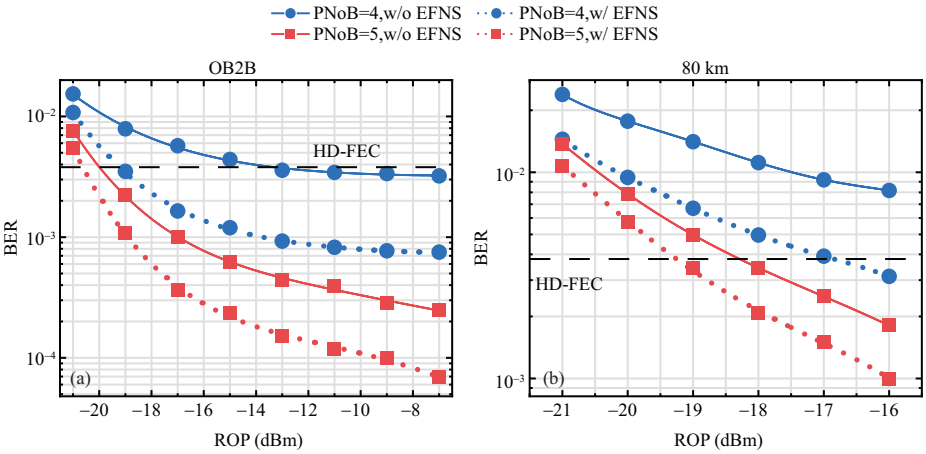

Figure 8 (Color online) ROP versus BER in the VCA-SSB 56-Gbit/s KK-16-QAM transmission. (a) OB2B transmission; (b) 80 km SSMF transmission.

5.2 VCA-SSB 60-Gbit/s KK-64-QAM transmission

Thanks to KK detection, advanced complex modulation formats are feasible in direct detection (DD) systems, such as 16-QAM and 64-QAM [7, 23]. In this subsection, we experimentally construct a VCA-SSB 60-Gbit/s KK-64-QAM transmission system to study the performance of EFNS on a KK detection system.

Figure 9 shows the results of CSPR versus BER for both OB2B and 80 km SSMF transmission. As shown in Figure 9(a), when EFNS was applied, the optimum CSPR for PNoB = 4 increased from 6.82 to 8.28 dB, increasing 1.46 dB, and the BER decreased from 3.0×10^{-2} to 8.8×10^{-3}, meeting the soft-decision forward error correction (SD-FEC) threshold. When PNoB = 5, applying EFNS, the optimal CSPR increased from 8.28 to 8.6 dB, increasing 0.32 dB. Furthermore, the BER decreased from 8.8×10^{-3} to 4.2×10^{-3}, and the CSPR required to reach the SD-FEC threshold was reduced by 0.2 dB. When PNoB = 8, the optimal CSPR was 8.91 dB, and the BER was 3.4×10^{-3}. The experimental results of the 80 km transmission are shown in Figure 9(b). When PNoB = 4, applying EFNS, the optimum CSPR increased from 8.28 to 8.92 dB, increasing 0.64 dB, and the BER reduced from 4.2×10^{-2} to 1.4×10^{-2}, meeting the SD-FEC threshold. When PNoB = 5, applying EFNS, the optimum CSPR increased from 8.92 to 9.52 dB, increasing 0.6 dB, and the BER decreased from 1.5×10^{-2} to 8.8×10^{-3}. The CSPR required to reach the SD-FEC threshold was reduced by 1 dB. In addition, with the help of EFNS, the BER performances at PNoB = 4 were very close to those at PNoB = 5 without EFNS enabled in both OB2B and 80 km transmission. When PNoB = 8, the optimal CSPR was 8.91 dB, and the BER was 8×10^{-3}.

Figure 10 shows the AWG output amplitude versus BER in OB2B and 80 km transmission. In Fig-

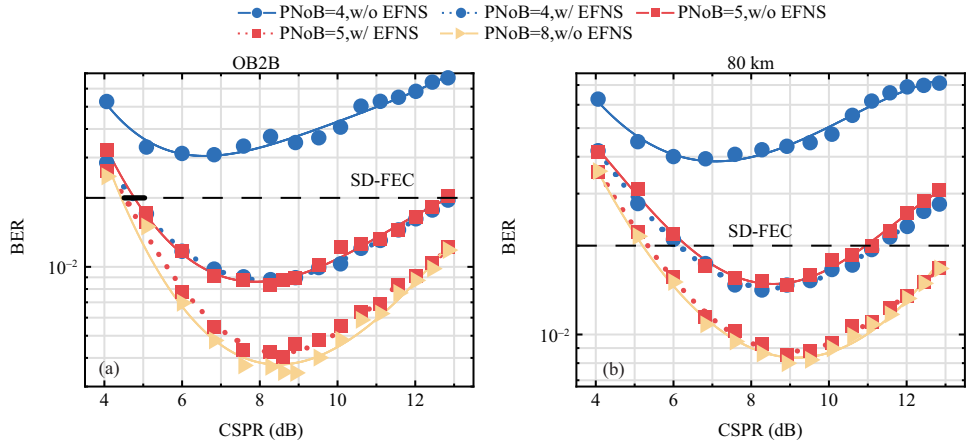

Figure 9 (Color online) CSPR versus BER in the VCA-SSB 60-Gbit/s KK-64-QAM transmission. (a) OB2B transmission; (b) 80 km SSMF transmission.

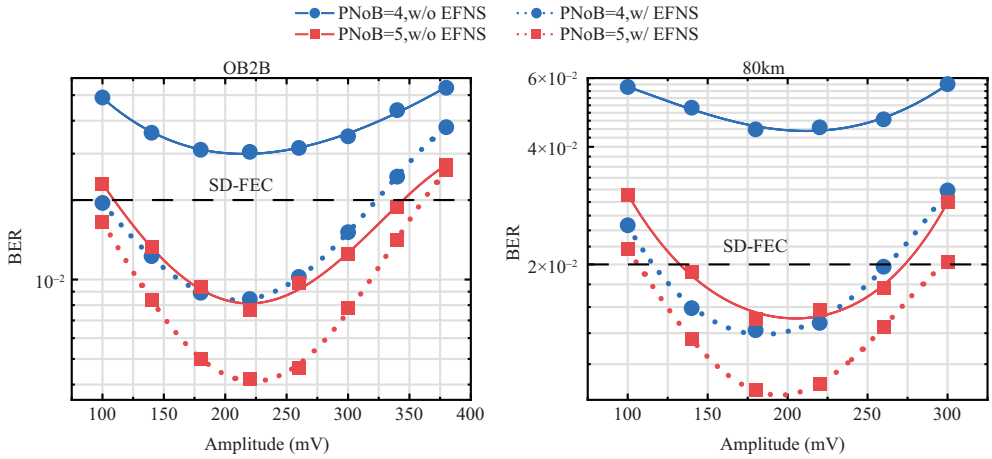

Figure 10 (Color online) AWG output amplitude versus BER in the VCA-SSB 60-Gbit/s KK-64-QAM transmission. (a) OB2B transmission; (b) 80 km SSMF transmission.

ure 10(a), when PNoB = 4, applying EFNS, the BER performance met the SD-FEC threshold. When PNoB = 5, applying EFNS, the maximum AWG output amplitude met the SD-FEC threshold, which is increased by 14 mV. As shown in Figure 10(b), in 80 km transmission, when PNoB = 4, applying EFNS, the BER performance met the SD-FEC threshold. When PNoB = 5, applying EFNS, the required AWG output amplitude at the SD-FEC threshold was reduced by 30 mV. The maximum AWG output amplitude for meeting the SD-FEC threshold was increased by 27 mV. The experimental results showed that the application of EFNS reduced the AWG output amplitude required by the KK detection system and improved the tolerance of nonlinear distortions on the transmitter side.

Figure 11 shows the ROP versus BER in OB2B and 80 km transmission. As shown in Figure 11(a), when applying EFNS, the BER performances at PNoB = 4 were very close to the one at PNoB = 5 without EFNS, and the required ROP at the SD-FEC threshold was −18.6 dBm. When PNoB = 5, applying EFNS, the required ROP was reduced by 1 dBm at the SD-FEC threshold. As shown in Figure 11(b), when applying EFNS, the BER performance at PNoB = 4 met the SD-FEC threshold. When PNoB = 5, applying EFNS, the required ROP was reduced by 1.1 dBm at the SD-FEC threshold.

The above experimental results of Subsections 5.1 and 5.2 indicate that in the KK detection system, the application of EFNS could not only improve the optimal CSPR of the system but also reduce the AWG output amplitude required for the FEC thresholds and improve the receiver sensitivity.

5.3 Synergistic effects of EFNS and KK detection

The synergistic effects of EFNS and KK detection imply that the application of the EFNS algorithm increases the optimal CSPR. The increased optimal CSPR leads to reduced SSBI and contributes to

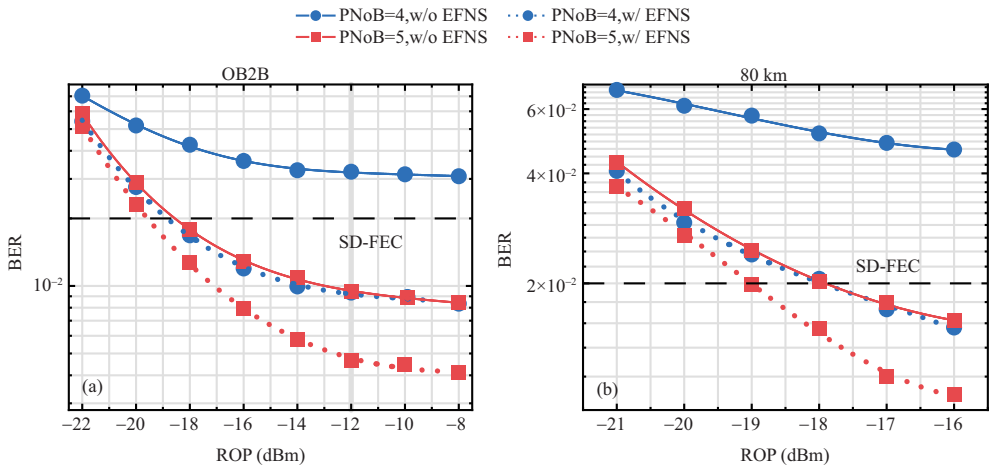

Figure 11 (Color online) ROP versus BER in the VCA-SSB 60-Gbit/s KK-64-QAM transmission. (a) OB2B transmission; (b) 80 km SSMF transmission.

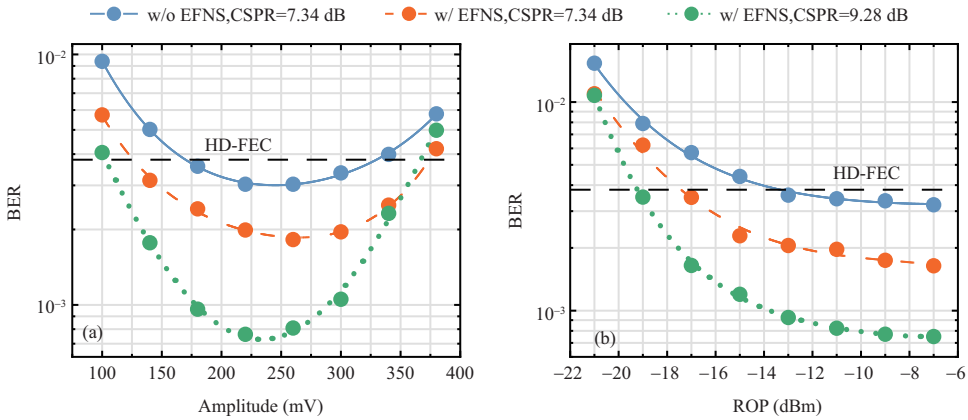

Figure 12 (Color online) Experimental results for VCA-SSB 56-Gbit/s KK-16-QAM OB2B transmission at PNoB = 4. (a) AWG output amplitude versus BER; (b) ROP versus BER.

the CFR, ultimately further enhancing system performance. Consequently, to investigate the synergistic effects of EFNS and KK detection on the system performance, we selected the cases of 16-QAM and 64-QAM OB2B transmission systems at PNoB = 4 for analysis. Three cases were analyzed:

Case 1. Under the optimal CSPR without EFNS, only the KK detection is employed in the transmission system.

Case 2. Under the optimal CSPR without EFNS, KK detection combined with EFNS is employed in the transmission system.

Case 3. Under the optimal CSPR with EFNS, KK detection combined with EFNS is employed in the transmission system.

Figure 12 shows the experimental results of VCA-SSB 56 Gbit/s KK-16QAM OB2B transmission at PNoB = 4, where 7.34 dB is the optimal CSPR without EFNS and 9.28 dB is the optimal CSPR with EFNS. As shown in Figure 12(a), when comparing Cases 1 and 2, the required amplitude was reduced by 44 mV at the HD-FEC threshold in Case 2. Comparing Cases 2 and 3, the required amplitude was reduced by 24 mV at the HD-FEC threshold in Case 3. Figure 12(b) shows that at the HD-FEC threshold, the ROP required for comparing Case 3 with Cases 1 and 2 was reduced by 5.9 and 1.8 dBm, respectively. The experimental results demonstrate that the application of EFNS not only enhanced the overall system performance but also improved the optimal CSPR to improve the capability of KK detection. This synergistic effect led to further enhancement of system performance.

Figure 13 shows the experimental results of VCA-SSB 60-Gbit/s KK-64-QAM OB2B transmission at PNoB = 4, where 6.82 dB was the optimal CSPR without EFNS and 8.28 dB was the optimal CSPR with EFNS. As shown in Figure 13, when PNoB = 4, with the help of EFNS, the BER performances met the SD-FEC threshold. Figure 13(a) shows that the BER performances in Case 2 were very close to

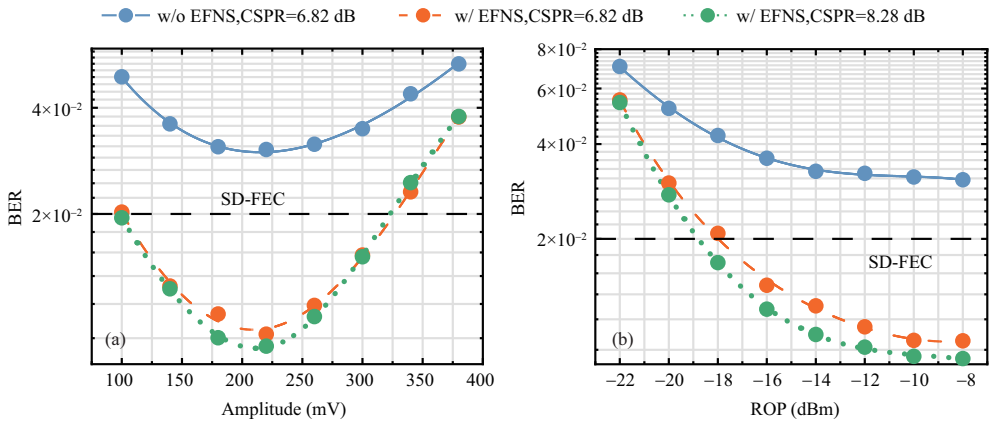

Figure 13 (Color online) Experimental results for VCA-SSB 60-Gbit/s KK-64-QAM OB2B transmission at the PNoB = 4. (a) AWG output amplitude versus BER; (b) ROP versus BER.

those in Case 3. Figure 13(b) shows that when comparing Cases 2 and 3, the required ROP was reduced by 0.8 dBm at the SD-FEC limit. Based on the experimental results shown in Figures 12 and 13, it can be observed that the impact of quantization noise on system performance was significantly greater in the KK-64-QAM OB2B transmission with PNoB = 4 compared to the KK-16-QAM OB2B transmission with the same PNoB. In this scenario, the application of EFNS played a vital role in enhancing system performance by reducing quantization noise. Although enabling EFNS also increased the optimal CSPR of KK detection and enhanced the reconstruction capability of the complex optical field, leading to performance improvement, its impact on system performance was relatively smaller compared to the improvement achieved by EFNS in mitigating quantization noise.

6 Conclusion

We delved into the effects of EFNS on a low-resolution KK detection system. First, we conducted a simulation-based analysis to investigate the efficacy of EFNS in mitigating the increased quantization noise resulting from the addition of the virtual carrier at the transmitter. Then, the VCA-SSB 56-Gbit/s KK-16-QAM and VCA-SSB 60 Gbit/s KK-64-QAM with the transmission of OB2B and 80 km at the PNoBs of 4, 5, and 8 were experimentally analyzed to demonstrate the effects of EFNS on the KK detection system. The experimental results showed that applying EFNS could improve the BER performance of the KK detection system compared to the case without EFNS and improved the optimal CSPR. Moreover, the required AWG output amplitudes at the FEC limit were reduced, and the receiver sensitivities were improved by applying the EFNS. When PNoB = 4, for 56-Gbit/s 16-QAM signals, the optimal CSPR was increased by 1.58 dB in 80 km transmission. The optimum CSPR was increased by 1.02 dB when PNoB = 5. For 60-Gbit/s 64-QAM signals, the optimum CSPR was increased by 0.64 dB in 80 km transmission when PNoB = 4. The optimal CSPR was increased by 0.6 dB when PNoB = 5.

Furthermore, we investigated the synergistic impact of EFNS and KK detection on system performance. The experimental results highlighted that the application of EFNS not only enhanced the overall system performance but also improved the capability of KK detection by increasing the optimal CSPR, thereby further boosting system performance.

Overall, EFNS showed excellent performance in the low-resolution KK detection system, demonstrating its great potential in low-cost, large-capacity optical communication systems.

Acknowledgements This work was supported by National Natural Science Foundation of China (Grant Nos. 61821001, 62371056) and Fund of State Key Laboratory of Information Photonics and Optical Communication BUPT (Grant No. IPOC2021ZT18).

References

1 Buscaino B, Taylor B D, Kahn J M. Multi-Tb/s-per-fiber coherent co-packaged optical interfaces for data center switches. J Lightwave Technol, 2018, 37: 3401–3412
2 Wang F, Yao H P, Zhang Q, et al. Dynamic distributed multi-path aided load balancing for optical data center networks. IEEE Trans Netw Serv Manage, 2022, 19: 991–1005
3 Krause Perin J, Shastri A, Kahn J M. Data center links beyond 100 Gbit/s per wavelength. Opt Fiber Tech, 2018, 44: 69–85
4 Mecozzi A, Antonelli C, Shtaif M. Kramers-Kronig coherent receiver. Optica, 2016, 3: 1220

5 Chen X, Antonelli C, Chandrasekhar S, et al. Kramers-Kronig receivers for 100-km datacenter interconnects. J Lightwave Technol, 2018, 36: 79–89
6 Shu L, Li J Q, Wan Z Q, et al. Single-lane 112-Gbit/s SSB-PAM4 transmission with dual-drive MZM and Kramers-Kronig detection over 80-km SSMF. IEEE Photon J, 2017, 9: 1–9
7 Shu L, Li J Q, Wan Z Q, et al. Single-photodiode 112-Gbit/s 16-QAM transmission over 960-km SSMF enabled by Kramers-Kronig detection and sparse I/Q Volterra filter. Opt Express, 2018, 26: 24564–24576
8 Li Z, Erkilinc M S, Shi K, et al. SSBI mitigation and the Kramers-Kronig scheme in single-sideband direct-detection transmission with receiver-based electronic dispersion compensation. J Lightwave Technol, 2017, 35: 1887–1893
9 Mecozzi A. A necessary and sufficient condition for minimum phase and implications for phase retrieval. 2016. ArXiv:1606.04861
10 Erkilinc M S, Thakur M P, Pachnicke S, et al. Spectrally Efficient WDM Nyquist pulse-shaped subcarrier modulation using a dual-drive mach-zehnder modulator and direct detection. J Lightwave Technol, 2016, 34: 1158–1165
11 Zhang Q, Stojanovic N, Prodaniuc C, et al. Demonstration of CD pre-compensated direct detection PAM4 40km transmission in C-band using DDMZM. In: Proceedings of the Asia Communications and Photonics Conference (ACP), Wuhan, 2016. 1–3
12 Zhu Y X, Zou K H, Chen Z Y, et al. 224 Gb/s optical carrier-assisted Nyquist 16-QAM half-cycle single-sideband direct detection transmission over 160 km SSMF. J Lightwave Technol, 2017, 35: 1557–1565
13 Sun C, Che D, Shieh W. Comparison of chromatic dispersion sensitivity between Kramers-Kronig and SSBI iterative cancellation receiver. In: Proceedings of the Optical Fiber Communications Conference and Exposition (OFC), San Diego, 2018. 1–3
14 Le S T, Schuh K, Chagnon M, et al. 1.72-Tb/s virtual-carrier-assisted direct-detection transmission over 200 km. J Lightwave Technol, 2018, 36: 1347–1353
15 Le S T, Schuh K, Chagnon M, et al. 8×256 Gbps virtual-carrier assisted WDM direct-detection transmission over a single span of 200 km. In: Proceedings of the European Conference on Optical Communication (ECOC), Gothenburg, 2017. 1–3
16 Lu D X, Lau A P T, Lu C, et al. Theoretical CSPR analysis and performance comparison for four single-sideband modulation schemes with Kramers-Kronig receiver. IEEE Access, 2019, 7: 166257
17 Shu L, Yu Z M, Sun K X, et al. Error-feedback noise shaping for low-resolution high-speed IM/DD and coherent transmission systems. In: Proceedings of the Optical Fiber Communications Conference and Exposition (OFC), San Francisco, 2021. 1–3
18 Shu L, Yu Z M, Sun K X, et al. Performance investigation of error-feedback noise shaping in low-resolution high-speed IM/DD and coherent transmission systems. J Lightwave Technol, 2022, 40: 3669–3680
19 Huang H Y, Yu Z M, Shu L, et al. Low-resolution optical transmission using joint shaping technique of signal probability and quantization noise. Chin Opt Lett, 2023, 21: 050602
20 Ling W A. Shaping quantization noise and clipping distortion in direct-detection discrete multitone. J Lightwave Technol, 2014, 32: 1750–1758
21 Schreier R, Pavan S, Temes G C. Understanding Delta-sigma Data Converters. Hoboken: Wiley, 2017. 27–61
22 Sun C, Che D, Ji H L, et al. Study of chromatic dispersion impacts on Kramers-Kronig and SSBI iterative cancellation receiver. IEEE Photon Technol Lett, 2019, 31: 303–306
23 Li Z, Erkilinc M S, Shi K, et al. Spectrally efficient 168 Gb/s/λ WDM 64-QAM single-sideband Nyquist-subcarrier modulation with Kramers-Kronig direct-detection receivers. J Lightwave Technol, 2018, 36: 1340–1346